6(2009) 363 – 383



Latin American Journal of Solids and Structures
www.lajss.org

Numerical and experimental analysis of yield loads in welded gap hollow YT-joint

Abstract

This paper presents an analytical, experimental, and numerical analysis of plain steel, circular hollow sections welded into a YT joint. The overall behavior and failure of the joint are characterized under axial compression of the lap brace. There are two joint failure modes: plastic failure of the chord face and local buckling of the chord walls. Numerical finite element models agree with the experimental data, in terms of principal stress near the joint intersection, with an accuracy of around 10%. The finite element model thus proves to be reliable and accurate, and will be used in future parametric studies.

Keywords

Hollow structures, joints, numerical analysis, experimental analysis.

R. F. Vieira[a,*], J. A. V. Requena[a], A. M. S. Freitas[b] and V. F. Arcaro[a]

[a] State University of Campinas, Campinas, SP – Brazil
[b] Federal University of Ouro Preto, Ouro Preto, MG – Brazil

Received 6 May 2009;
In revised form 1 Oct 2009

* Author email: rosilenefv@gmail.com

1 INTRODUCTION

One of the reasons that steel structures are used more frequently in buildings nowadays is that their manufacturing process presents several economic advantages. In this context, the increasing demand for hollow sections worldwide must be pointed out; they have provided many buildings with an elegant and modern look. Thus, one of the factors that determine the cost of steel structures is the manufacturing of standardized hollow sections.

The most common hollow sections have square (SHS-Square Hollow Sections), rectangular (RHS-Rectangular Hollow Sections), or circular cross sections (CHS-Circular Hollow Sections). They are made of highly resistant steel, the yield stress is around 350MPa. One of the companies that manufacture this material in Brazil is VALLOUREC & MANNESMANN TUBES, or V&M do BRASIL S.A. (formerly Mannesmann S.A.). It was founded in 1953 at the request of the Brazilian government, to meet the growing demand of their oil industry.

The first stage of this study characterizes the behavior of welded joints constructed from structural hollow sections under the criteria suggested by EUROCODE 3 [3], Packer and Handerson [6], Packer et al. (CIDECT 1992) [7] and Wardenier et al. (CIDECT 1991) [8]. On this basis, we created a prototype YT joint by welding circular hollow sections. The second stage involved mechanical testing of this prototype. The experimental program involves four YT joints tested to analyses the behavior, failure modes, displacements and stress distribution.

NOMENCLATURE

A_i	cross sectional area of member i $(i = 0, 1, 2, 3)$
E	modulus of elasticity
E_t	modulus of elasticity tangent
M_0	bending moment in the chord member
N_i	axial force applied to member i $(i = 0, 1, 2, 3)$
N_i^*	joint design resistance expressed in terms of axial load in member i
N_{0P}	pre-stressing axial force on the chord
W_0	elastic section modulus of member i $(i = 0, 1, 2, 3)$
d_i	external diameter of circular hollow section for member i $(i = 0, 1, 2, 3)$
e	nodding eccentricity for a connection
f_y	yield stress
f_{yi}	yield stress of member i $(i = 0, 1, 2, 3)$
f_{0P}	pre-stress in chord
$f(n)$	function which incorporates the chord pre-stress in the joint resistance equation
g	gap between the bracings members of a K, N or KT joint, at the face of the chord
g'	gap divided by chord wall thickness
n'	$\frac{f_{0P}}{f_{y0}} = \frac{N_{0P}}{A_0 \cdot f_{y0}} + \frac{M_0}{W_0 \cdot f_{y0}}$
t_i	thickness of hollow section member i $(i = 0, 1, 2, 3)$
β	diameter ratio between bracing on chord
	$\beta = \frac{d_1}{d_0}, \frac{d_1}{b_0}, \frac{b_i}{b_0}$ T, Y and X
	$\beta = \frac{d_1+d_2}{2 \cdot d_0}, \frac{d_1+d_2}{2 \cdot b_0}, \frac{b_1+b_2+h_1+h_2}{4 \cdot b_0}$ K and N
γ	ratio of the chord's half diameter to its thickness
ν	poisson's ratio
θ	included angle between bracing member i $(i = 0, 1, 2, 3)$ and the chord
ϵ	maximum specific proportionality strain
f	stress
f_{lp}	maximum proportionality stress
f_r	maximum resistance stress
f_1	principal stress 1
f_2	principal stress 2

The third stage of this study uses Ansys [2] to model the hollow joints as an assembly of SHELL elements. The experimental results were used to calibrate the numerical model.

2 FAILURE MODES JOINTS

A great deal of experimental research has been done on welded hollow sections to show the various modes of failure that can occur. The result depends on the joint type, load conditions, and many other geometrical parameters. There are several formulations describing the failure modes: some derive from theoretical studies, while others are merely empirical models. Packer

and Handerson [6] presents the failure modes of bracing K-joints in square and rectangular hollow sections. They are: MODE A – plastic failure of the chord face; MODE B – punching shear failure of the chord face; MODE C – tension failure of the web member; MODE D – local buckling of the web member; MODE E – overall shear failure of the chord; MODE F – local buckling of the chord walls; and MODE G – local buckling of the chord face.

3 CALCULATION OF CONNECTION RESISTANCE

The YT joint prototype design uses the methodology presented by Wardenier et al. (CIDECT 1991) [8] and Packer and Henderson [6].

The Fig. 1 shows forces general scheme using as a limit the maximum capacity of the vertical brace member of the YT joint and the bending moment due the eccentricity was not considered.

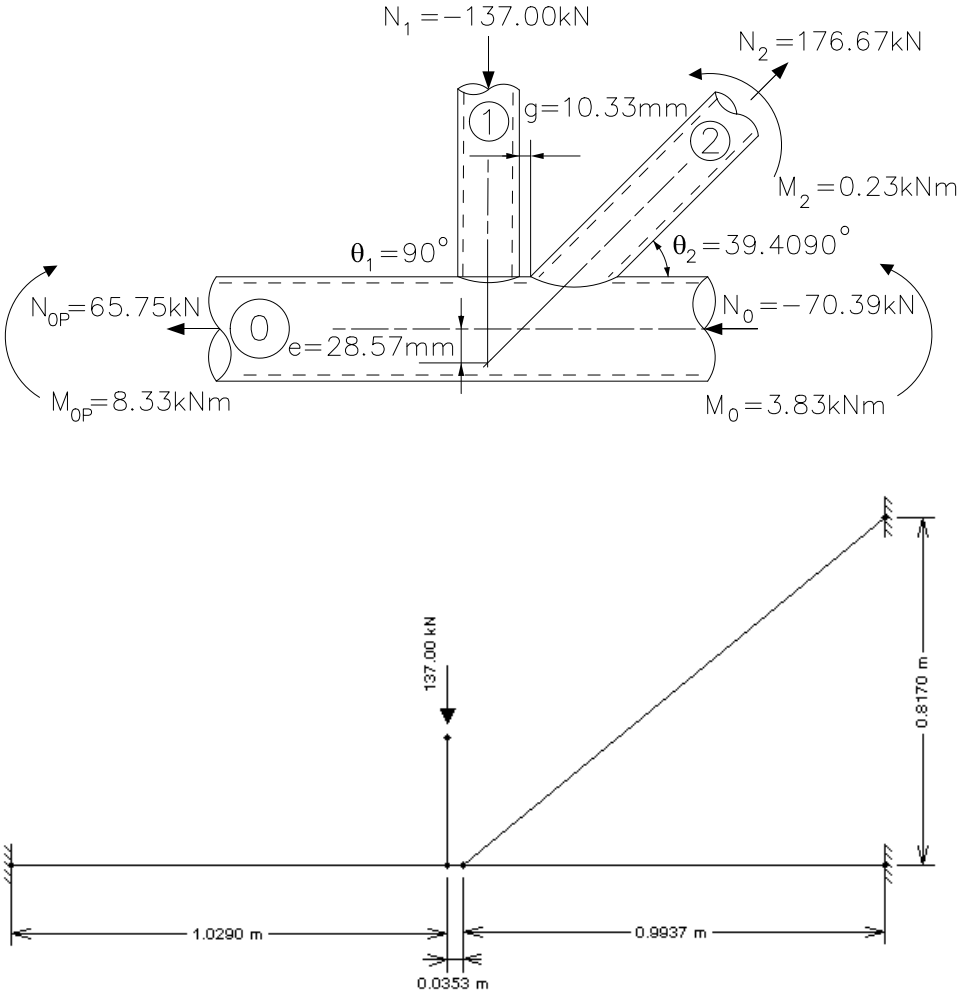

Figure 1 Forces general scheme of YT joint.

Table 1 shows the geometric characteristics of the VMB 250 circular hollow sections used in the YT joint. The nominal physical proprieties yield stress (f_y) are equal 250 MPa.

Table 1 Physical and geometrical characteristics.

Member	Hollow Section	Thickness	Area	Elastic resistant modulus	Load
	mm	mm	mm^2	mm^3	kN
Chord	ϕ114.3	#6.02	2047.83	52677.51	N_0 = - 70.39 N_{0P}= 65.75
Lap brace	ϕ73.0	#5.16	1099.73	17433.30	N_1= -137.00
Through brace	ϕ73.0	#5.16	1099.73	17433.30	N_2=176.67

3.1 Validity limits

The YT joint meets all geometrical requirements described in the aforementioned references.

3.2 Calculations

a) YT joint parameters

The YT joint parameters are given by Eq. (1) through Eq. (5):

$$\beta = \frac{d_1 + d_2}{2 \cdot d_0}; \tag{1}$$

$$g' = \frac{g}{t_0}; \tag{2}$$

The stress on the chord, f_{0P}, depends most critically on the compressing stress.

$$n' = \frac{f_{0P}}{f_{y0}} = \frac{N_{0P}}{A_0 \cdot f_{y0}} + \frac{M_0}{W_0 \cdot f_{y0}}; \tag{3}$$

$$f(n') = 1.0 + 0.3 \cdot n' - 0.3 \cdot n'^2 \leq 1; \tag{4}$$

$$f(\gamma, g') = \gamma^{0.2} \cdot \left(1 + \frac{0.024 \cdot \gamma^{1.2}}{1 + \exp^{(0.5 \cdot g' - 1.33)}}\right); \tag{5}$$

b) Plastic failure of the chord face (Mode A)

Vertical lap brace:

$$N_1^* = \frac{f_{y0} \cdot t_0^2}{sen\theta_1} \left(1.8 + 10.2 \cdot \frac{d_1}{d_0}\right) \cdot f\ (\gamma, g')\ \cdot\ f\ (n')\ ; \tag{6}$$

Diagonal through brace:

$$N_2^* = N_1^*\ \cdot \left(\frac{sen\theta_1}{sen\theta_2}\right); \tag{7}$$

c) Punching shear failure of the chord face (Mode B)

Vertical lap brace and diagonal through brace are both given by Eq. (8):

$$N_i^* = \frac{f_{y0} \cdot t_0 \cdot \pi \cdot d_i}{\sqrt{3}}\ \cdot \left(\frac{1 + sen\theta_i}{2 \cdot sen^2\theta_i}\right); \tag{8}$$

d) YT Joint Resistance

The joint resistance is the lowest value obtained in items (b) and (c) above.
Vertical lap brace:

$$\frac{N_1}{N_1^*} < 1; \tag{9}$$

Diagonal through brace:

$$\frac{N_2}{N_2^*} < 1; \tag{10}$$

Table 2 presents the results of the calculation.

Table 2 Results of the calculation procedure.

Joint parameters	**Acronym**	**Calculation**
Relation between diameters	β	0.64
Relation between diameter and thickness	γ	9.49
n'=stress/f_y (compression)	n'	-0.14
Function of prestress on chord	f(n')	0.95
Resistance plastic failure of the chord face (Mode A)	N_1^*(Pl)	137.40 kN
Resistance punching shear failure of the chord face (Mode B)	N_1^*(Pu)	199.27 kN
Lap brace use	N_1/N_1^*	1.0
Resistance plastic failure of the chord face (Mode A)	N_2^*(Pl)	216.42 kN
Resistance punching shear failure of the chord face (Mode B)	N_2^*(Pu)	404.16 kN
Through brace use	N_2/N_2^*	0.82

4 EXPERIMENTAL PROGRAM

To study the joint, it was first necessary to determine the mechanical properties of the material through test-body traction. Then four prototypes constructed from seamless rolled tubes were manufactured by V&M do Brasil. They were called pre-experiment, experiments I, II and III.

4.1 Traction test

A stress-strain diagram was obtained through test-body traction measurements [1].

Table 3 presents data obtained from the stress-strain diagram. The flp term is defined as the stress that corresponds to a strain of approximately 0.0012 [5].

Table 3 Data provided by the stress-strain diagram.

Test Bodies	ϵ	f_{lp}	f_y	f_r	E
	X10-6	MPa	MPa	MPa	MPa
cp1a - ϕ73mm	1199	259.3	314.5	480.3	216222.8
cp1b - ϕ73mm	1165	220.3	326.0	486.9	189114.6
cp2a - ϕ114.3mm	1062	323.2	332.2	465.1	304461.5
cp2b - ϕ114.3mm	1165	264.9	322.6	473.6	227390.8

4.2 YT joint prototypes

The dimensions of the prototypes are shown in Fig. 2. The prototypes are fixed by four screws at each end. They were loaded axially at the top of the lap brace.

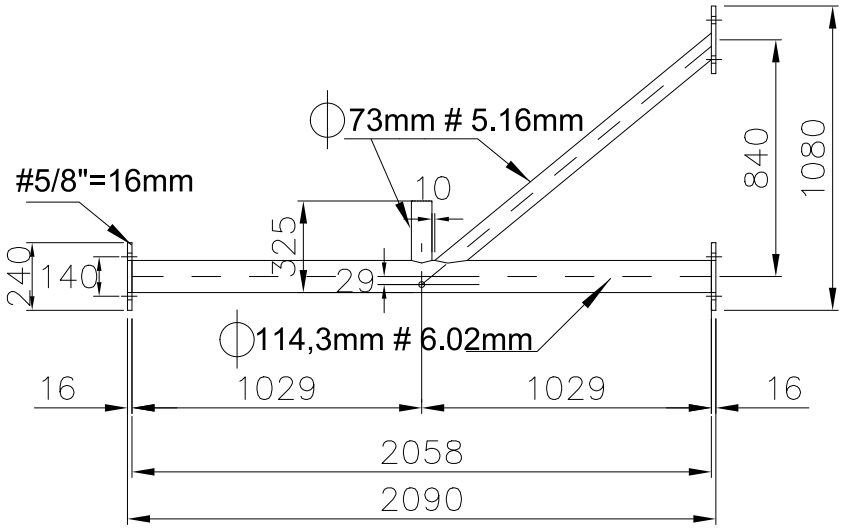

Figure 2 YT joint prototype (mm).

4.3 Instrumentation for tests

In EXPERIMENTS I, II and III, sixteen 5mm electrical resistance KFG-5-120-C1-11 extensometers were used. Their positions are marked EER1 to EER16 in Fig. 3.

The EERs were placed on the prototype to measure longitudinal strain, drawing on the work of FUNG et al [4]. In EXPERIMENT III, 2 rosette gauges and 2 individual extensometers were added (for a total of 24 EERs). Rosette 1 was composed of EER20, EER21 and EER22; rosette 2 was composed of EER17, EER18 and EER19. EER23 and EER24 were placed at the bases of the lap brace and through brace respectively.

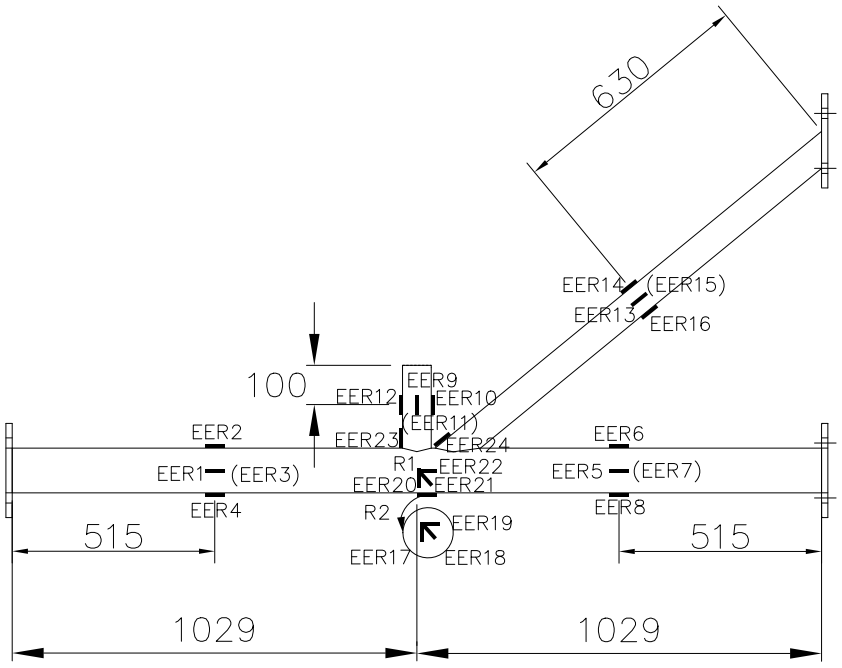

Figure 3 Positioning of the extensometers on the YT joint prototype.

In EXPERIMENTS I, II and III, 19 manual reading displacement transducers (TD1 to TD19) and two digital reading displacement transducers (TD20 and TD21) were placed on the prototype as shown in Fig. 4.

4.4 Experimental results

The testing methodology used was defined in three stages, as shown below:

- **Stage I** - Before starting the test, the prototype was subjected to a cycle of 10 loading of approximately 20% of the estimated collapse loading for the connection, to minimize friction and check the torque of the screws. Based on pre-test the loading was estimated at 50kN. This level of loading is within the elastic limit of the material. The force was applied in small increments and then it was done downloading.

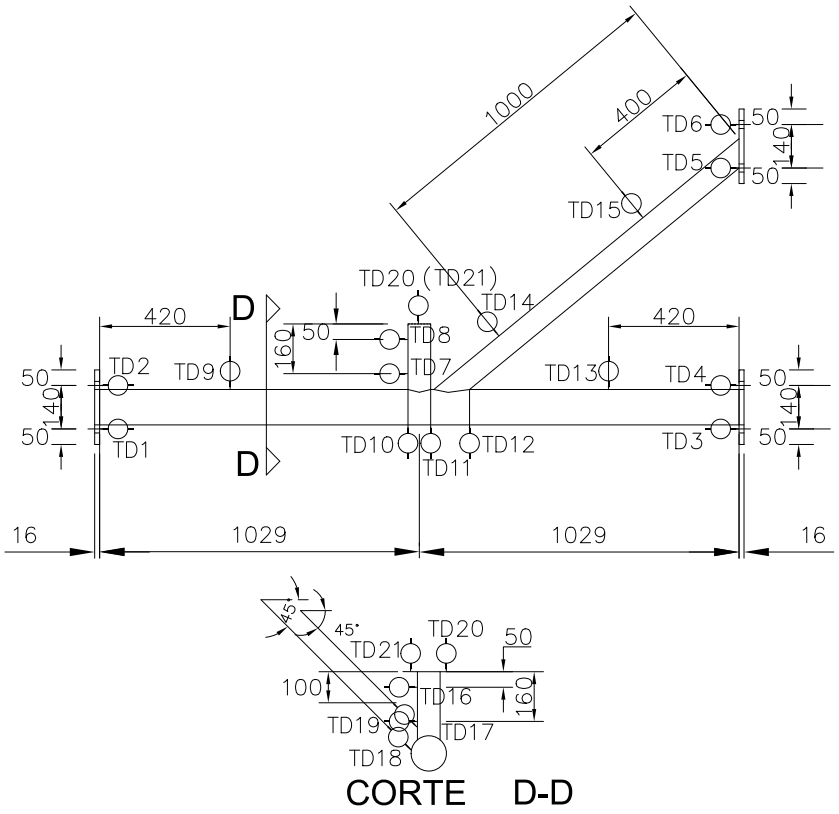

Figure 4 Positioning of the DTs on the YT joint prototype.

- **Stage II** - During the test the speed of the actuator load was kept as slow and steady as possible for both the case of loading and for unloading. The step load was previously set depending on the stage supposed to loading. At each step of loading, when the pre established loading was reached, expected time to stabilize the transducers and then did the reading.

- **Stage III** - The prototype was loaded to the ultimate state, where the prototype did not offer more resistance, even after he reached the break. Then the prototype was unloaded.

Fig. 5 shows the overall strain of the prototype in EXPERIMENT III, characterized by the development of failure Mode A.

Fig. 6 shows a more detailed photograph of the failure mechanism in EXPERIMENT II.

The Fig. 7 shows local buckling of the chord intersection, characteristic of failure Mode F.

The results presented by extensometers in each EXPERIMENTS I, II and III are similar, are representing the state of tension expected for each region and thus show that the tests were equivalent.



Figure 5 Overall strain of the prototype for EXPERIMENT III.



Figure 6 Failure Mode A: plastic failure of the chord face at EXPERIMENT II.



Figure 7 Failure Mode F: local buckling of the chord face.

The results of the last loading for each of the tests are shown in Table 4.

Table 4 Last loading to EXPERIMENTS I, II and III.

EXPERIMENTS	**Last loading (kN)**
EXPERIMENT I	240,0
EXPERIMENT II	358,6
EXPERIMENT III	316,4

Two failure modes were observed: plastic failure of the chord face (Mode A) and local buckling of the chord walls (Mode F).

4.5 Presentation and analysis of the test results

The extensometers provide similar data in each experiment, and correspond to the expected stress levels at each location. The displacement transducers reported little displacement of the members. Plastic strain occurred mainly near the joint intersection, where rosette 1 was placed.

5 ANALYSIS OF FINITE ELEMENTS

Two numerical models were created in Ansys, one using a bilinear stress-strain diagram (BISO – Bilinear Isotropic Hardening) and the other a multilinear (piecewise linear) diagram (MISO – Multilinear Isotropic Hardening). Their results were compared to the experimental tests.

Both physical and geometrical non-linearity were considered in the analysis. To implement physical non-linearity, we used the stress-strain diagrams obtained in our traction test of the prototype (Section 4.1).

The contour conditions were simulated in Ansys through displacement restrictions. Force was applied in an increasing way, that is, at unit load pitches.

Fig. 8 and Fig. 9 show the stress-strain diagrams of test bodies selected for the numerical analysis. The multilinear model is represented by 26 points (crossed circles), and the bilinear model by two straight lines (triangles).

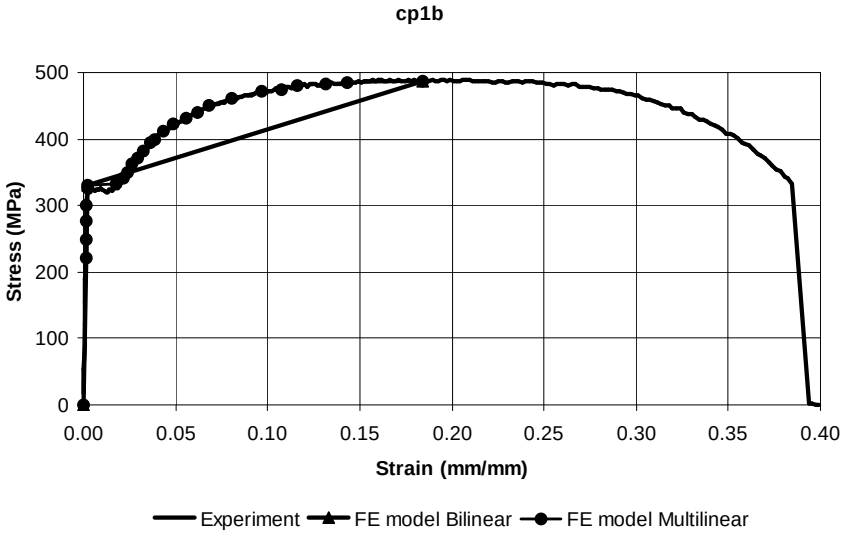

Figure 8 Experimental, bilinear and multilinear stress-strain diagrams used for test body cp1b, from the through brace and lap brace (ϕ73mm).

Table 5 shows data used to represent the material properties of test bodies cp1b and cp2b in the numerical model. Note that the bilinear stress-strain diagram always runs from the origin to the first stress peak (f), then from this point to the maximum stress (fr) of the material.

Table 5 Data used to represent the bilinear stress-strain diagram with the Ansys software (BISO).

Test Body	**fy**	**f**	**fr**	**E**	**Et**
	MPa	MPa	MPa	MPa	MPa
cp1b(ϕ73mm)	326.0	331.1	486.9	189114.6	856.5
cp2b(ϕ114.3mm)	322.6	322.6	473.6	227390.8	840.6

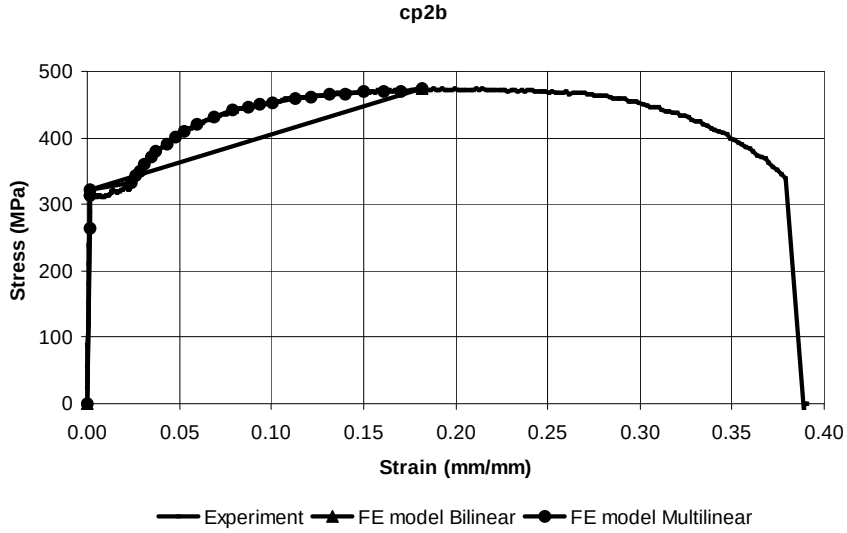

Figure 9 Experimental, bilinear and multilinear stress-strain diagrams used for test body cp2b, from the chord (ϕ114,3mm).

The 26 points to represent the multilinear stress-strain diagram is shown by Table 6.

Table 6 Data used to represent the multilinear stress-strain diagram with the Ansys software (MISO).

Points	cp1b(ϕ73mm)			cp2b(ϕ114,3mm)		
	e	**f**	**E**	**e**	**f**	**E**
	Dimensionless	GPa	GPa	Dimensionless	GPa	GPa
0	0	0	0	0	0	0
1	0.001165	0.22031	189.1146	0.001165	0.2649	227.3908
2	0.0013373	0.24958	186.6298	0.0014234	0.31285	219.7906
3	0.0015613	0.27689	177.3458	0.0017508	0.32257	184.2415
4	0.0017853	0.29975	167.899	0.023651	0.33273	14.06833
5	0.001992	0.32604	163.6747	0.026081	0.34245	13.13025
6	0.0022849	0.3311	144.9079	0.028562	0.3501	12.25754
7	0.017672	0.3324	18.80942	0.031181	0.3607	11.56794
8	0.021394	0.34219	15.99467	0.034834	0.37027	10.62956
9	0.023668	0.35058	14.8124	0.037418	0.38073	10.17505
10	0.026442	0.36218	13.69715	0.043173	0.39133	9.06423
11	0.029286	0.3713	12.67841	0.047722	0.40085	8.39969
12	0.032646	0.38115	11.67524	0.052478	0.41042	7.820801
13	0.036229	0.39585	10.92633	0.059905	0.42068	7.022452

(continued)

Table 6 Data used to represent the multilinear stress-strain diagram with the Ansys software (MISO) *(continuation)*.

Points	cp1b(ϕ73mm)			cp2b(ϕ114,3mm)		
	e	**f**	**E**	**e**	**f**	**E**
	Dimensionless	GPa	GPa	Dimensionless	GPa	GPa
14	0.038728	0.40007	10.33025	0.068554	0.43103	6.287452
15	0.043656	0.41183	9.433526	0.0786	0.44115	5.612595
16	0.048567	0.42287	8.706941	0.0874737	0.44546	5.092552
17	0.055838	0.43131	7.72431	0.093987	0.45077	4.796089
18	0.061989	0.44038	7.104164	0.1006035	0.45302	4.50305
19	0.068227	0.4504	6.601492	0.11285	0.46019	4.077891
20	0.080736	0.46188	5.720868	0.12118	0.46171	3.810117
21	0.096589	0.47179	4.884511	0.13124	0.465	3.543127
22	0.1074614	0.47472	4.417572	0.14001	0.46647	3.331691
23	0.1159	0.48035	4.144521	0.15042	0.46932	3.120064
24	0.1316533	0.48221	3.662694	0.1611	0.4701	2.918063
25	0.14347	0.48564	3.384959	0.17035	0.47025	2.760493
26	0.18417	0.48688	2.643644	0.18148	0.47364	2.609874

The Poisson's ratio was obtained by compression test tube used. The value obtained was ν=0.3.

The SHELL element was considered most appropriate to represent hollow structures. Specifically, the SHELL181 element was used to generate a mesh for the hollow sections. The SHELL63 element was used for fixation plates. Table 7 shows their characteristics.

Table 7 Characteristics of elements.

Elements	**Nr of nodes per element**	**Degrees of freedom**	**Special features**		
SHELL 63	4	6	Elastic	Large deflection	Little strain
SHELL 181	4	6	Plastic	Large deflection	Large strain

Fig. 10 shows the finite element model of the YT joint prototype. Fig. 11 shows the principal stress (f1) of the multilinear model. Fig. 12 shows the initial position of the strained joint in more detail.

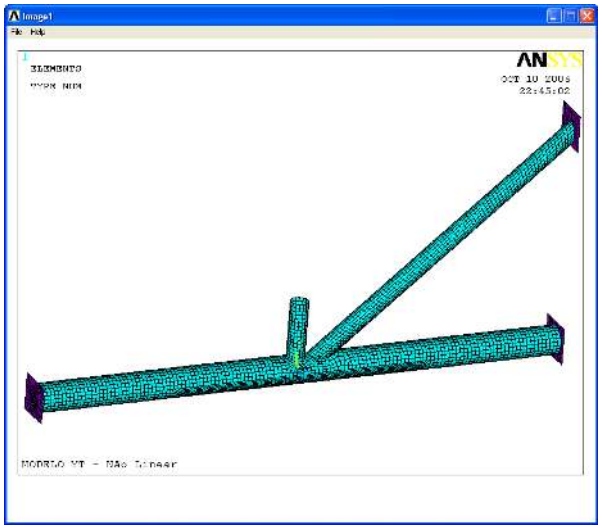

Figure 10 Finite element model of the YT joint prototype.

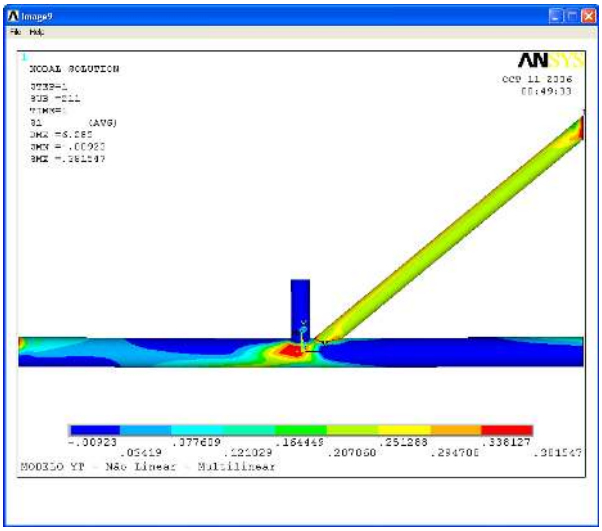

Figure 11 Principal stress (f1) for the multilinear model (GPa).

6 COMPARISON BETWEEN EXPERIMENTAL TEST RESULTS AND NUMERICAL MODEL RESULTS

The experimental tests and numerical models can be compared on the basis of strains obtained by the extensometers.

In EXPERIMENT II several loading and unloading cycles were carried out, with slight strain occurring in each cycle. In this case, we only report the results of the last cycle. This is why the readings reported for EXPERIMENT II do not present zero initial strain.

The results are divided according to location: chord, lap brace, through brace and rosette.

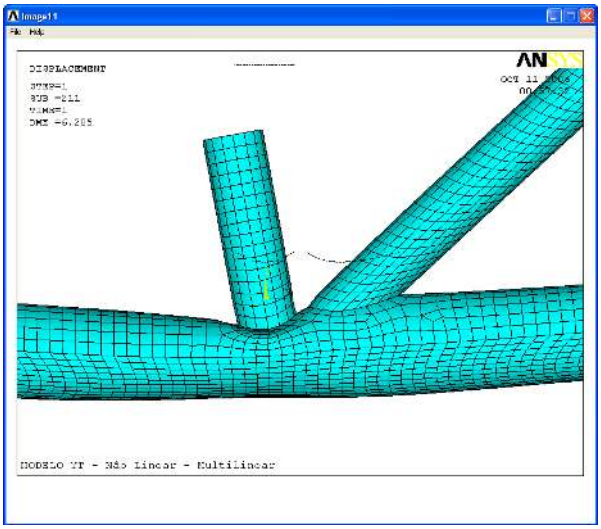

Figure 12 Detail of the multilinear model strain.

The strain on the chord was recorded by extensometers EER1 to EER8. These points do not represent plastic strain. In this paper, only the results from extensometers EER1, EER2 and EER4 are presented (Fig. 13, Fig. 14 and Fig. 15 respectively).

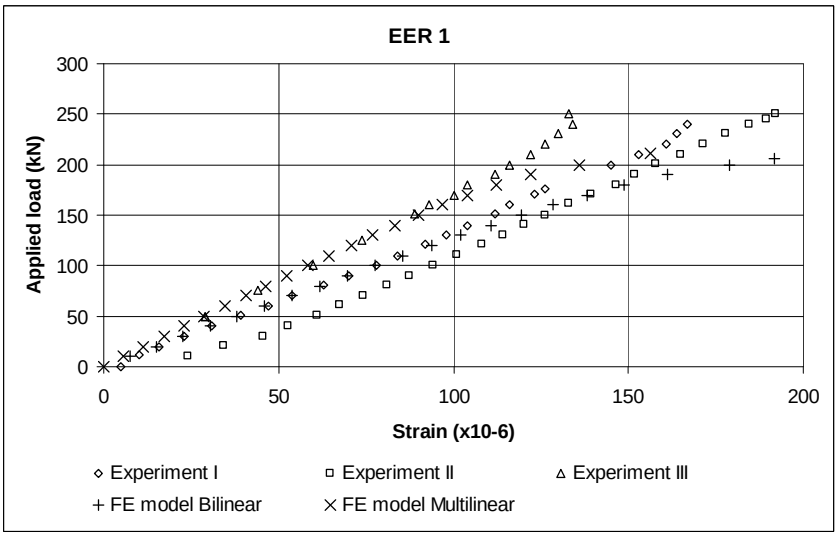

Figure 13 Chord strain recorded by extensometer EER1 and the numerical models.

The inversion of strain in Fig. 14 indicates the mechanism of failure Mode A.

For the compressed lap brace, extensometers EER9 to EER12 and EER23 provide very similar results. Only the result from EER9 is shown here, in Fig. 16.

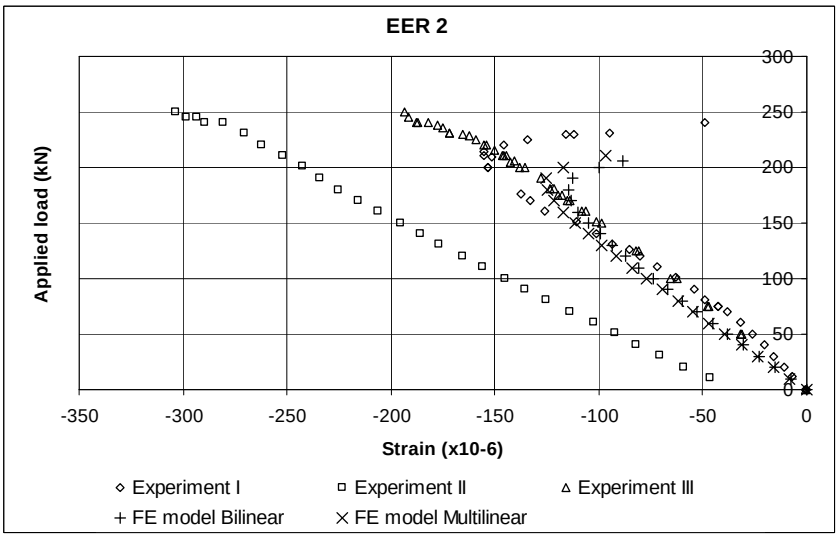

Figure 14 Chord strain recorded by extensometer EER2 and the numerical models.

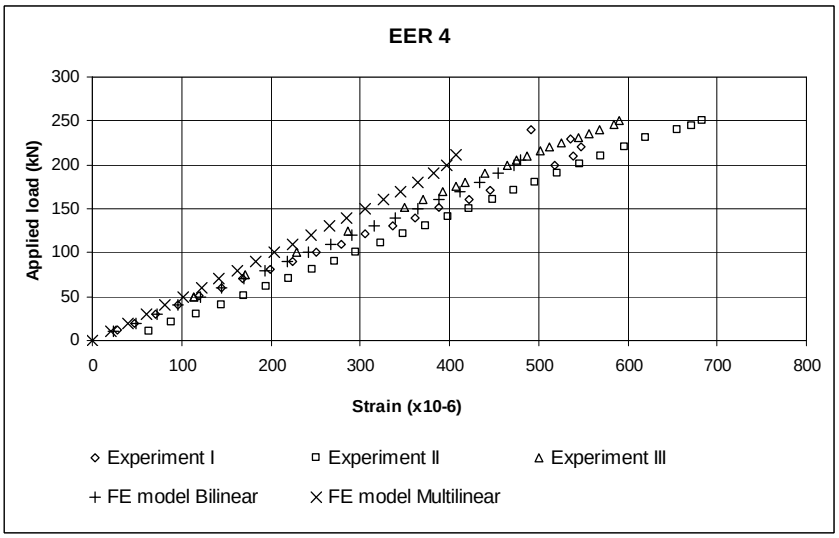

Figure 15 Chord strain recorded by extensometer EER4 and the numerical models.

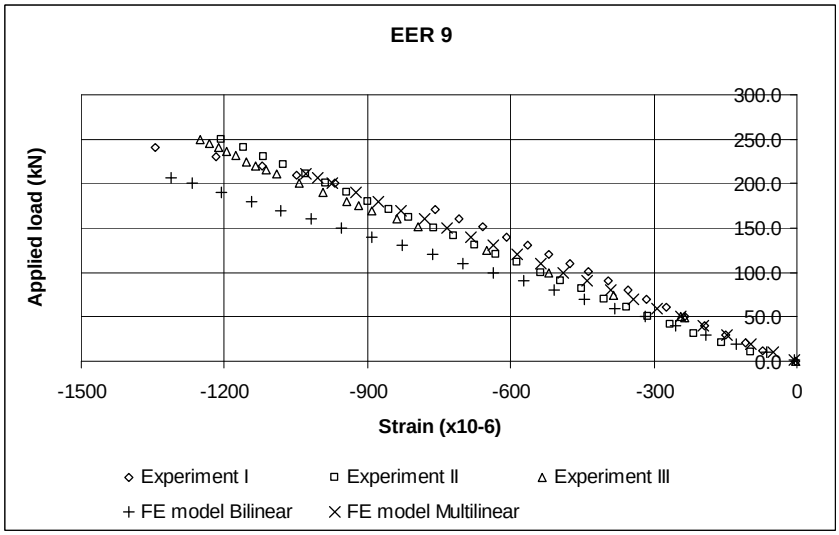

Figure 16 Lap brace strain recorded by extensometer EER9 and the numerical models.

For the through brace, only the result from EER13 is shown (Fig. 17).

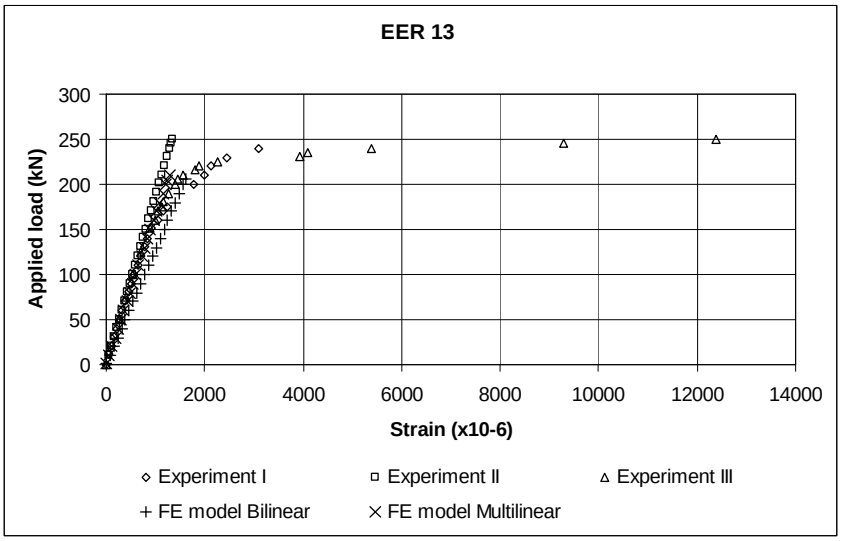

Figure 17 Through brace strain recorded by extensometer EER13 and the numerical models.

Measurements were also done with a caliper rule to characterize the local buckling of the chord face measured in EXPERIMENTS I and II. These data were compared to the displacement in the multilinear numerical model. The result is shown in Fig. 18.

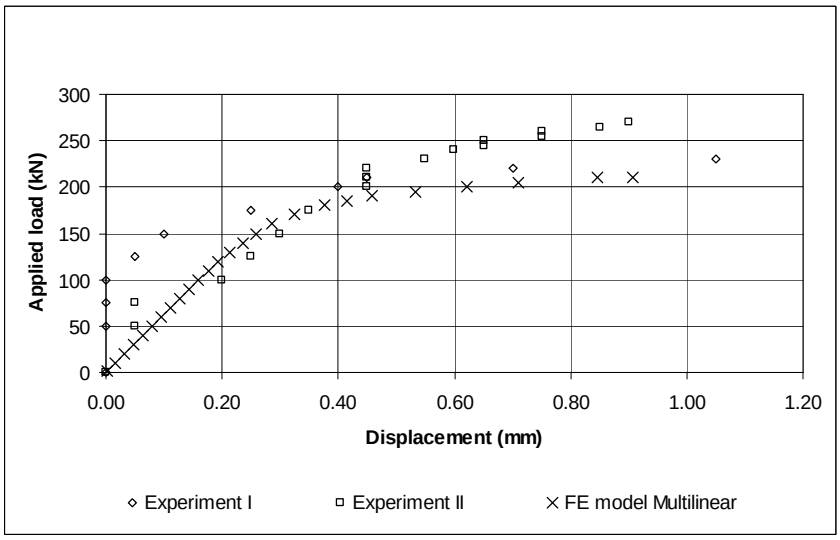

Figure 18 Local buckling of the chord face.

As for the rosettes, comparisons between theory and experiment can be made between the principal stresses.

Fig. 19 and Fig. 20 show the principal stresses f_1 and f_2 measured at rosette 1 in EXPERIMENT III and the numerical models.

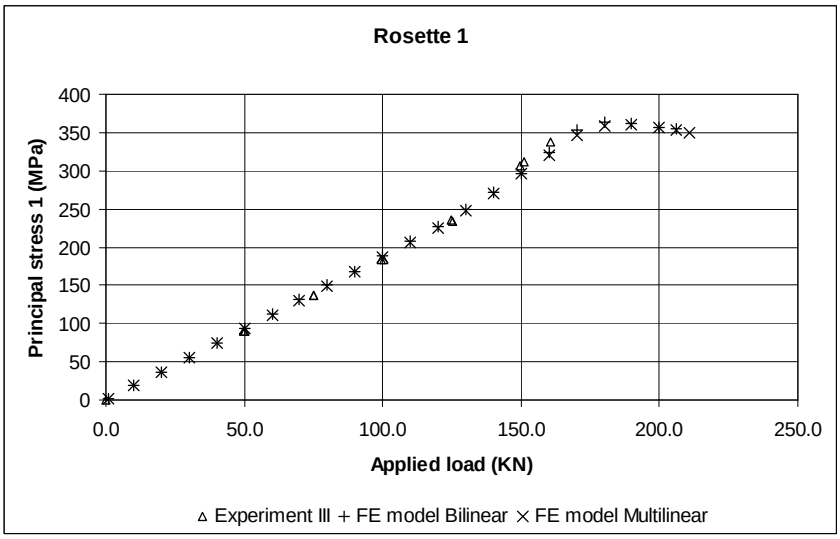

Figure 19 Principal stress f_1 measured at rosette 1 in EXPERIMENT III and the numerical models.

The principal stresses f_1 and f_2 of the two numerical models were in good agreement with those obtained by rosette 1 in EXPERIMENT III.

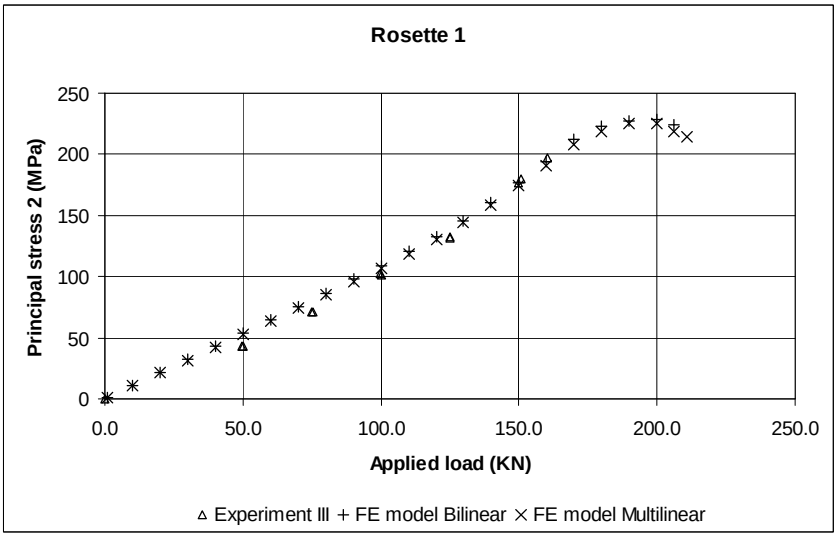

Figure 20 Principal stress f_2 measured at rosette 1 in EXPERIMENT III and the numerical models.

7 CONCLUSION

The experimental tests and numerical analysis agree that the most critical region of the joint is its intersection, where the greatest stress concentration is found. At this spot there was plasticization.

For each of the hollow sections, the yield stress f_y can be obtained by finding the average of the stresses provided during the traction test. The average yield stress of the chord is 330 MPa.

The yield load of the YT joint is whatever load induces the yield stress in at least one section.

The yield load measured by rosette 1 in EXPERIMENT III may not be the yield load of the YT joint, however, because the yield may have occurred at some other point. Still, it must be very close as numerical models identify this area as having the greatest stress concentration.

With numerical modeling, it is possible to obtain the yield load at the location corresponding to rosette 1. It also provides the real yield load of the finite element model, which can be compared to the yield load of the real YT joint. Table 8 shows the relative error between the principal stresses f1 obtained by numerical models and rosette 1 in EXPERIMENT III. The error is only around 10%, which is quite good.

In the numerical models, the yield load was found by examining all nodes in the chord area corresponding to rosette 1. We took the load on whichever node reached the yield stress (f_y=330 MPa) first. The results are shown in Table 9.

According to international technical rules the measuring load for this joint is 137kN, not considering the contribution of the bending moment. The yield loads provided by numerical modeling are 17.5% greater than the measuring load, which shows that the formulation presented by Wardenier et al. (CIDECT 1991) [8] and PAcker and Henderson [6] is safe for these

Table 8 Error percentage of the principal stress, f_1, for the spot represented by rosette 1 and the Ansys numerical models.

Load (kN)	**Experiment III**	**FE model Bilinear**	**FE model Multilinear**	**Error Bilinear**	**Error Multilinear**
	f_1**(Mpa)**	f_1**(Mpa)**	f_1**(Mpa)**		
50.0	90.4	93.3	92.7	3.1	2.5
75.0	136.6	140.4	139.4	2.7	2.0
100.2	183.5	188.0	186.6	2.4	1.7
125.0	233.1	237.3	236.1	1.8	1.3
151.0	311.5	298.3	297.3	4.4	4.8
160.4	346.6	323.1	319.7	7.3	8.4
170.0	376.6	352.9	345.9	6.7	8.9
174.8	399.4	361.0	353.4	10.6	13.0

Table 9 Yield load for the Ansys numerical models.

	Yield Load(kN)
"Bilinear Ansys"	160
"Multilinear Ansys"	161

sections.

Both numerical models present good agreement with the experimental data, proving that physical non-linearity is not a determining factor for results.

There structure exhibited linear behavior until the load reached 157kN, at which point plastic strain started to occur.

The multilinear numerical model will serve as the basis for our next study, which will analyze the influence of the gap on the joint resistance.

Acknowledgements The authors are grateful for the support from UNICAMP, from Vallourec & Mannesmann Tubes (V&M do Brasil) and Prof. Flávio Costa.

References

[1] American Society for Testing and Materials - ASTM. Standart test methods for tension testing of metallic materials. Technical report, 1995.

[2] ANSYS Inc. *Theory reference, version 9.0.* 2004.

[3] Eurocode 3. Design of steel structures. part 1.1: General rules and rules for buildings, annex k. Technical Report Env 1993-1-1, 1992.

[4] T.C. Fung, C.K. Soh, W.M. Gho, and F. Qin. Ultimate capacity of completely overlapped tubular joints – I. An experimental investigation. *Journal of Constructional Steel Research*, 57(8):855–880, 2001.

[5] R.C. Hibbeler. *Resistência dos materiais*. Prentice Hall, São Paulo, 2004.

[6] J.A. Packer and J.E. Henderson. *Hollow structural section joints and trusses: a design guide*. Canadian Institute of Steel Construction, Ontario, 2nd edition, 1997.

[7] J.A. Packer, J. Wardenier, Y. Kurobane, D. Dutta, and N. Yeomans. *Design guide for rectangular hollow section (RHS) joints under predominantly static loading - CIDECT*. Verlag TÜV Rheinland Gmbtt, 1992.

[8] J. Wardenier, Y. Kurobane, J.A. Packer, D. Dutta, and N. Yeomans. *Design guide for circular hollow section (CHS) joints under predominantly static loading - CIDECT*. Verlag TÜV Rheinland Gmbtt, 1991.